Classical and semiclassical calculations of electron transfer cross sections in keV-energy ion-molecule collisions

J. Caillat,[1] A. Dubois,[1] I. Sundvor,[2] and J.-P. Hansen[2]
[1]*Laboratoire de Chimie Physique-Matière et Rayonnement, Université Pierre et Marie Curie, F-75231 Paris Cedex 05, France*
[2]*Institute of Physics, University of Bergen, N-5007 Bergen, Norway*
(Received 18 February 2004; published 27 September 2004)

We apply a many-body classical model and a semiclassical coupled-channel approach to study the electronic processes occurring in the course of fast collisions between atomic and molecular species. The methods are applied in a comparative study of electron transfer in $He^{2+}/Ar^{2+}-H_2^+$ collisions at keV u^{-1} impact energies. The classical calculations are in agreement with recent experimental data [H. Bräuning *et al.*, J. Phys. B **34**, L321 (2001)] for projectile velocities larger than the initial electron velocity. The semiclassical model is based on the sudden approximation where the electronic wave function is expressed by linear combinations of traveling atomic capture states and target molecular states obtained at fixed nuclei. The related charge transfer cross sections are slightly underestimated (overestimated) for He^{2+} (Ar^{2+}) when considering H_2^+ in its initial vibrational ground state. These cross sections do, however, depend strongly on the internuclear distance of the hydrogen molecular ion: when involving an initial vibrational excitation of the target, the averaged cross sections obtained from the semiclassical approach become in fair agreement with experiments.

DOI: 10.1103/PhysRevA.70.032715 PACS number(s): 34.10.+x, 34.50.Gb, 34.70.+e

I. INTRODUCTION

Scattering experiments between charged particles and molecules have displayed a range of interesting few-body phenomena involving coherent interplay between electrons and nuclei. That is true over the entire range of impact energies, from slow (eV) to very fast (MeV) collision regimes. Restricting the discussion to nonreactive scattering, experimental studies of dissociative electron transfer, vibronic excitation, correlation, isomer effects, and post-collisional interaction effects are some of the most representative examples; see, e.g., [1–12] and references therein. For diatomic molecules electronic emission spectra have recently shown interference phenomena resulting in oscillatory relative double-differential cross sections [13–15]. Note that scattering events with selected molecular orientation can also be analyzed indirectly, or potentially directly [16], through coincidence measurements and analysis of molecular fragment anisotropy distributions [5,9], Fundamental collision studies are also of direct relevance for applications—for example, in astrophysical- or atmospheric-related phenomena—since, e.g., transport phenomena depend nonlinearly on electronic cross sections [17].

On the theoretical side, the development of *ab initio* theories has not followed the same rapid progress as experimental studies, partly because dynamical charged many-body problems become exponentially more complex with increasing number of nuclei. Except from pure quantal approaches designed for cold and thermal collisions—e.g. [18–20],—various semiclassical approaches have been applied; cf. among others the review of Gislason *et al.* [21] and recent coupled wave packet treatments [22]. These methods utilize partial decoupling of the electronic and nuclear motions, and can thus efficiently describe vibronic phenomena and dissociative electron transfer. These methods are, however, limited to impact energies of about 100 eV u^{-1} and below.

For higher collision energies the problem can be very awkward. First, an increasing number of electronic channels, including ionization, has to be included. Second, the relative momentum of the electron with respect to both reactants should be taken into account, as in ion-atom collisions [23,24]. However, in this intermediate-energy regime elucidating simplifications can be used. By decoupling completely the electronic and nuclear degrees of freedom of the molecule, the quantal problem reduces to the description of the dynamics of the electronic cloud in the field of fixed molecular nuclei, in the presence of one traveling charged particle. At low collision energies corresponding to velocities lower or equal to the classical electron velocity ($v \leqslant v_e$), theory has advanced based on the static molecular multicenter problem, followed by an expansion of the wave function in a molecular-state basis [25,26]. In the high-energy limit the transfer cross sections have been evaluated through linear combinations of probability amplitudes or matrix elements stemming from pure ion-atom calculations associated with each atom of the molecule [15,27–29]. At intermediate energies this approach cannot be validated since the electron dynamics is strongly coupled to all nuclei involved in the collision process.

Alternatively, in the intermediate to high-energy regime, classical approaches have been developed quite successfully to collisions between simple molecules and protons or multiply charged ions; cf., for example [30–32], and references therein. These treatments are similar to their counterparts in ion-atom collisions, but require further approximations to deal with the extra repulsive terms related to the nucleus-nucleus and electron-electron interactions within the molecular target. To get rid of these intrinsic difficulties, an alternative classical method has been developed [33,34] and applied recently to antiproton and muon collisions with hydrogen molecules [35].

In this paper we present results for collisions between He^{2+} and Ar^{2+} projectiles and H_2^+ molecular ions in the en-

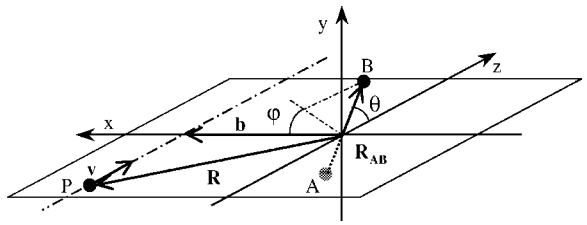

FIG. 1. Collision geometry in the laboratory fixed reference frame: the projectile velocity ($\vec{v}$) and the impact parameter vector ($\vec{b}$) define a collision plane. The angles θ and φ define the orientation of the target molecular axis $\vec{R}_{AB}$ with respect to the z axis and the collision plane.

ergy range around maximum electron transfer cross sections. We first present results from the classical model developed in [33,35], hereafter referred to as the Kirschbaum-Wilets-Cohen (KWC) model. Then we introduce a semiclassical scheme for ion-molecule scattering based on asymptotic correct molecular and atomic states, in principle valid from about 100 eV u^{-1} to MeV u^{-1} collision energies. We especially address effects related to the initial H_2^+ vibrational excitation and compare the results of the two models with experimental results of Bräuning *et al.* [36]. Atomic units are used unless otherwise stated.

II. THEORETICAL MODELS

The heavy-particle coordinates and the collision geometry are displayed in Fig. 1. The projectile (P) trajectory is described by the impact parameter $\vec{b}$ and velocity $\vec{v}$, parallel to the quantization z axis. The orientation of the diatomic molecule (represented by the centers A and B) is defined by the angle θ with respect to the beam direction ($\vec{v}$) and the azimuthal angle φ which refers to the $(\vec{b},\vec{v})$ collision plane. The electronic coordinates $\vec{r}$, not shown in the figure, are defined with respect to the midpoint of the H_2^+ internuclear distance.

A. Classical KWC model

A classical many-body model for use in atomic collisions was introduced by Kirschbaum and Wilets [33] in 1980. Their model provides a framework for atomic collisions where, in addition to the usual kinetic energy and Coulomb potential terms, two kinds of momentum-dependent potentials are added to the Hamiltonian of the target. One of these two-body potentials (so-called *Pauli* constraint) acts between electrons with identical spin. The purpose is to mimic to some degree a shell structure for many-electron systems. The other type of potential is motivated by the fact that the electrons should not be allowed to collapse onto the nucleus (the so-called *Heisenberg* constraint). These two extra repulsive potentials allow the classical stability of atomic ground-state configurations [33,37].

For molecules this model gives also a stable ground-state configuration. A problem is, however, that it does not give the correct binding energy of the electron(s), even for simple molecules as H_2 and H_2^+ [33]. Cohen [38] found that this was due to a symmetric placement of the electron(s) in the molecules; for example, in the case of H_2^+, the electron is put in the middle of the two nuclei. A method to avoid this was introduced by Cohen through additional potential energy terms in the Hamiltonian so that the molecule gets the correct ground-state energy for any internuclear distance. The model developed by Cohen is well documented in his paper [38]; we are going to outline only the main features of the model as it is implemented in our context.

In the KWC model, the target Hamiltonian corresponding to the hydrogen molecular ion does not include Pauli constraint terms and is written as

$$H_T = H_0 + W_{Ae}^{(\xi)} + W_{Be}^{(\xi)} + W_{Oe}^{(\xi')}, \tag{1}$$

where H_0 is the physical Hamiltonian with kinetic energies and Coulomb potentials and the three other terms are the extra repulsive Heisenberg constraint potentials acting between the electron and, respectively, the nuclei A, B and the midpoint O between A and B. The effective potentials $W_{ij}^{(\xi)}$ are of the form $r^{-2}f(rp)$ where r and p are the relative distance and momentum between the two particles i and j. The term $W_{Oe}^{(\xi')}$ is similar, with r replaced by the internuclear distance R_{AB} in front of the function $f(rp)$. The function $f(rp)$ is given as

$$f(rp) \equiv \frac{(\hbar\xi)^2}{4\alpha} \exp\left\{ \alpha\left[1 - \left(\frac{rp}{\hbar\xi} \right)^4 \right] \right\}, \tag{2}$$

where the stiffness constant α is set equal to 4, as in [38]: large enough to make the W terms small in H_T without creating numerical instabilities in the dynamical calculations. The parameters ξ and ξ' were obtained by Cohen through a minimization scheme in order to have a correct electronic ground-state energy of H_2^+ at equilibrium distance $R_{AB,eq}$. We have chosen the values of these parameters as well as the configuration in position and momentum spaces as they are listed in Table I of [38]. Note that any random rotation around the internuclear axis and inversion with respect to the midpoint O may be applied to give a set of initial conditions for the molecular target in the collision simulations.

To describe the collision, the projectile kinetic term plus all Coulombic attractive and repulsive terms between P and A,B and the electron are added to the target Hamiltonian H_T. Hamilton's equations of motion corresponding to the four-body system are then solved numerically, exactly as in the usual classical trajectory Monte Carlo (CTMC) method developed for ion-atom collisions [39]. This model describes simultaneously all possible electronic processes as well as the molecular target rotation, vibration, and dissociation during the collision stage. Note also that when bound particles dissociate due to the perturbation, the extra terms included in the Hamiltonian vanish [as $f(rp) \to 0$ when $r \to \infty$; cf. Eq. (2)] and the particles propagate in the only Coulomb field from the other charged particles. Finally, the integral cross sections for inelastic processes are evaluated from a statistically relevant set of initial conditions [24,40].

B. Semiclassical (2+1)-center theory

In the energy regime under consideration here (typically $0.1-100$ keV u^{-1}) which corresponds to subfemtosecond collision times, all inelastic channels are open and coupled. Therefore a nonperturbative description of the dynamics of the electronic charge cloud delocalized on the three centers is required. However, in this impact velocity range, the relative motion of the different heavy particles may be decoupled from the electronic degrees of freedom. The treatment may then be considerably simplified by assuming (i) the rovibrational *sudden* approximation—i.e., frozen molecular internuclear vector $\vec{R}_{AB}$ [21]—and (ii) a classical straight-line description of the projectile-target relative motion, $\vec{R}=\vec{b}+\vec{v}t$. For one-electron systems, the Hamiltonian can then be written as

$$H = -\frac{1}{2}\Delta_{\vec{r}} + V^T(\vec{r};\vec{R}_{AB}) + V^P(r_P(t)), \tag{3}$$

where $\vec{r}_P(t)=\vec{r}-\vec{R}(t)$, V^P is the potential related to the electron-projectile subsystem and, V^T is the two-center potential experienced by the electron with respect to the molecular target, e.g., for H_2^+:

$$V^T(\vec{r};\vec{R}_{AB}) = -\frac{1}{\left|\vec{r}-\frac{1}{2}\vec{R}_{AB}\right|} - \frac{1}{\left|\vec{r}+\frac{1}{2}\vec{R}_{AB}\right|}. \tag{4}$$

Within this approach, we have developed a new coupled-channel code to solve the time-dependent Schrödinger equation for the electronic scattering states expressed as

$$\Psi(\vec{r},t) = \sum_k c_k^T(t)\phi_k^T(\vec{r};\vec{R}_{AB})e^{-iE_k^T(R_{AB})t} + \sum_{k'} c_{k'}^P(t)\chi_{k'}^P(\vec{r}_P(t))e^{-i\varepsilon_{k'}^P t}F(\vec{r},t). \tag{5}$$

Note that this ansatz defines a $(2+1)$-center theory for collisions between diatomic molecules and atomic ions:

(i) The molecular two-center nature of the target is exactly described by static diatomic molecular orbitals (MO's), ϕ_k^T (of energy E_k^T) depending parametrically on $\vec{R}_{AB}$ and expressed as linear combinations of atomic orbitals centered on A and B:

$$\phi_k^T(\vec{r};\vec{R}_{AB}) = \sum_i^{N_A} a_{k,i}^A\chi_i^A(\vec{r};\vec{R}_{AB}) + \sum_j^{N_B} a_{k,j}^B\chi_j^B(\vec{r};\vec{R}_{AB}). \tag{6}$$

(ii) Charge transfer processes are described by traveling asymptotic atomic orbitals (AO's) centered on the projectile, $\chi_{k'}^P$ (of energy $\varepsilon_{k'}^P$). Thus in this asymptotic representation of the total scattering wave function, the electronic translational factors (ETF), $F(\vec{r},t)$ remain unambiguously [42] described by plane waves $\exp(i\vec{v}\cdot\vec{r}-iv^2t/2)$, as in the semiclassical AO close-coupling approach developed for ion-atom collisions [24,41,43].

This procedure allows for the description of all kinds of inelastic scattering events, including ionizing collisions, and it opens for studying electronic time development in detail. Application of the time-dependent variational principle [24,44] to the expansion given in Eq. (5) leads to a set of coupled differential equations for the amplitudes, $\mathbf{c}=\{c_k^T(t);c_{k'}^P(t)\}$,

$$i\mathbf{S}(t)\frac{d}{dt}\mathbf{c}(t) = \mathbf{M}(t)\mathbf{c}(t). \tag{7}$$

The matrices $\mathbf{S}(t)$ and $\mathbf{M}(t)$ are overlap and coupling matrices in which the computationally demanding two-center elements take the form

$$S_{ji}^{TP}(t) = \langle\phi_j^T|\chi_i^P e^{i\vec{v}\cdot\vec{r}}\rangle e^{-i(\varepsilon_i^P+v^2/2-E_j^T)t}, \tag{8}$$

$$M_{ji}^{PT}(t) = \langle\chi_j^P e^{i\vec{v}\cdot\vec{r}}|H-E_i^T|\phi_i^T\rangle e^{-i(E_i^T-\varepsilon_j^P-v^2/2)t}. \tag{9}$$

The set of coupled equations (7) is solved in three steps: (i) determination of the projectile and target states by diagonalization of the projectile and target Hamiltonians, (ii) calculation of the overlap and coupling matrix elements on a fixed time grid, and (iii) numerical solution of the equations for given initial conditions $\mathbf{c}(t\to-\infty)$, impact parameter, and velocity.

1. Target and projectile orbitals

To describe the projectile and the target in a (pseudo-)one-electron picture, we have chosen to implement for V^T and V^P [see Eq. (3)] pure Coulombic potentials or model potentials of the form

$$V^X(r) = \sum_i \alpha_i r^{n_i} e^{-\beta_i r}, \tag{10}$$

where the n_i are integer (typically -1 and 0) and the variational parameters β_i are set to get correct atomic or molecular characteristics, ionization and/or binding energies, e.g., [45,46]. Such monocentric potentials are convenient for the description of the atomic projectile and the molecular target, when, in the latter case, terms centered on A and B (nuclei + core electrons) are used. The target and projectile states are then obtained by diagonalizing their individual Hamiltonian by using sets of Slater-type orbitals (STO's) centered, respectively, on one and two centers. The sets of states created by this variational procedure contain well-described ground and first excited states as well as loosely bound and ionization pseudostates. This representation is well suited for pure Coulombic systems and optimal in terms of the size of the basis sets for pseudo-one-electron systems. However, concerning the evaluation of multicenter integrals, such a kind of expansion is not efficient and we have therefore adopted a mixed representation of the projectile and target states. Each atomic and molecular STO-built state $[\mathcal{S}_j(r)]$ is fitted in terms of a sum $[\mathcal{G}_j(r)]$ of Gaussian-type orbitals (GTO's); this procedure involves a systematic optimization of the exponents of each GTO [47–49] by minimization of the integral, $\Delta_j = \int_0^{+\infty} r^2 dr[\mathcal{S}_j(r)-\mathcal{G}_j(r)]^2$.

2. Matrix elements

We shall now focus on the methods for the computation of the matrix elements, the stage which demands most of the

CPU time in the simulations. This requires the evaluation of one-, two-, and three-center integrals, with or without ETF's. In the present version of the code, all integrals involving one and two centers without ETF's are computed with the STO representation of the states, since their evaluations do not present any significant problem and are rather fast [50].

However, the evaluation of the two-center and three-center matrix elements with ETF's [cf. Eqs. (8) and (9)] requires extensive computational efforts when the states are expressed as STO expansions [51]. In this case, we use the GTO representation of the states and any of these integrals can be computed from the following general form:

$$I^g = \int_{-\infty}^{+\infty} dx \int_{-\infty}^{+\infty} dy \int_{-\infty}^{+\infty} dz\; r^{m1} r'^{m_2} r''^{m_3} x^{u_1} y^{v_1} z^{w_1} x'^{u_2} y'^{v_2} z'^{w_2} \times \frac{\exp(-\alpha_1 r^2 - \alpha_2 r'^2 - \alpha_3 r''^2 + i\mu \vec{v}\cdot\vec{r})}{(r'')^{\lambda}} \quad (11)$$

$$(\lambda = 0,\ 1\mu = 0, \pm 1).$$

In the present notations, (x,y,z) are the Cartesian coordinates of the electron position $\vec{r}$ relative to a given nucleus and $\vec{r}' = \vec{r} - \vec{\rho}$ and $\vec{r}'' = \vec{r} - \vec{\rho}'$ where $\vec{\rho}$ and $\vec{\rho}'$ can be any internuclear relative positions. The integers $u_1, v_1, \ldots, w_2$ and the even integers m_1, m_2, m_3 must be positive or zero. The very general form (11) stands for two- ($\vec{\rho}' = \vec{\rho}$) and three-center integrals, including a potential operator ($\lambda = 1$) or not ($m_3 - \lambda = 0, \alpha_3 = 0$), with or without ETF's (respectively, $\mu = \pm 1$ or 0). The integrals I^g can be written as

$$I^g = \lim_{\vec{a}\to\mu\vec{v}} \lim_{\vec{d}\to\vec{0}} \left(-i\frac{\partial}{\partial a_x}\right)^{u_1} \left(-i\frac{\partial}{\partial a_y}\right)^{v_1} \left(-i\frac{\partial}{\partial a_z}\right)^{w_1} \times \left(-i\frac{\partial}{\partial d_x}\right)^{u_2} \left(-i\frac{\partial}{\partial d_y}\right)^{v_2} \left(-i\frac{\partial}{\partial d_z}\right)^{w_2} \times \left(-\frac{\partial}{\partial \alpha_1}\right)^{m_1/2} \left(-\frac{\partial}{\partial \alpha_2}\right)^{m_2/2} \left(-\frac{\partial}{\partial \alpha_3}\right)^{m_3/2} J^g_{\lambda}, \quad (12)$$

with kernel integrals as

$$J^g_{\lambda} = \int_{-\infty}^{+\infty} dx \int_{-\infty}^{+\infty} dy \int_{-\infty}^{+\infty} dz \frac{e^{-\alpha_1 r^2 - \alpha_2 r'^2 - \alpha_3 r''^2 + i\vec{a}\cdot\vec{r} + i\vec{d}\cdot\vec{r}'}}{(r'')^{\lambda}} \quad (\lambda = 0,1). \quad (13)$$

The integral J^g_{λ} can be expressed analytically as

$$J^g_1 = \frac{2\pi^{3/2}}{B\sqrt{\alpha}}\, e^{-\alpha_2\rho^2 - \alpha_3\rho'^2 - i\vec{d}\cdot\vec{\rho}} e^{A^2/4\alpha}\, \mathrm{Erf}\left(\frac{B}{2\sqrt{\alpha}}\right), \quad (14)$$

$$J^g_0 = \left(\frac{\pi}{\alpha}\right)^{3/2} e^{-\alpha_2\rho^2 - i\vec{d}\cdot\vec{\rho}} e^{A^2/4\alpha} \quad (15)$$

where $\alpha = \alpha_1 + \alpha_2 + \alpha_3$, $\vec{A} = i(\vec{a} + \vec{d}) + 2\alpha_2\vec{\rho} + 2\alpha_3\vec{\rho}'$, $\vec{B} = \vec{A} - 2\alpha\vec{\rho}'$, and Erf($z$) is the complex error function. In practice, the successive derivations of J^g_{λ} are performed symbolically directly in the collision code, leading to a large number of terms, simple to evaluate numerically since including only powers of A, B, α_1, α_2, α_3, α, ρ, ρ_x, ρ_y, ρ_z, ρ', ρ'_x, ρ'_y, ρ'_z, v, v_x, v_y, v_z, exponentiations, the error function, and its derivatives. No numerical integration has to be performed so that the computations are very fast; this compensates the increase of the number of orbitals when going from STO's to GTO's. Note that this algorithm is not new (cf., for example, [52,53]), but the present implementation has the advantages of being general to any angular momentum and to control numerical instabilities.

3. Propagation stage and the cross sections

The coupled differential equations (7) are solved using a predictor-corrector algorithm [54] for a given set of fixed parameters: impact parameter, velocity, target internuclear distance and orientation ($\vec{R}_{AB}$), and the initial conditions given by the initial state i of the electron, bound by convention to the target,

$$\Psi(\vec{r}, t \to -\infty) = \phi_i^T(\vec{r}; \vec{R}_{AB}). \quad (16)$$

During the propagation, the matrix $-i\mathbf{S}^{-1}\mathbf{M}$ is evaluated at any time t by interpolation of the matrix elements values computed on a fixed time grid. The numerical quality of the expansion coefficients $\mathbf{c}(t)$ obtained asymptotically when the collision is over ($t \to +\infty$, practically when R is large enough so that the results are converged) can be checked by using the norm conservation and time-symmetry relations [55]. From the coefficients $c_k(t \to +\infty)$ we obtain the probabilities for any process $i \to f$, $P_{if}(b, R_{AB}, \theta, \varphi) = |c_f(t \to +\infty)|^2$, where we mention explicitly the dependence on the initial (and fixed) molecular alignment (θ, φ; cf. Fig. 1). The cross sections are then defined as

$$\sigma_{if}(R_{AB}, \theta) = \int d^2\vec{b} P_{if}(b, R_{AB}, \theta, \varphi) \quad (17)$$

and alignment averaged cross sections as [56]

$$\sigma_{if}(R_{AB}) = \frac{1}{2}\int_0^{\pi} \sin\theta d\theta \sigma_{if}(R_{AB}, \theta). \quad (18)$$

A treatment of the vibrational degrees of freedom within the sudden approximation can be found in [57,58]. When vibrational distributions are not resolved in the final channels, a sum over all, discrete and dissociative, vibrational states is performed and leads to the closure relation. The cross sections are then simply averaged over the distribution $|\psi_\nu(R_{AB})|^2$ for a given initial vibrational ψ_ν state:

$$\sigma_{if}^{(\nu)} = \int_0^{\infty} dR_{AB} |\psi_\nu(R_{AB})|^2 \sigma_{if}(R_{AB}). \quad (19)$$

Within the Franck-Condon approximation the cross sections (19) for a molecular target initially in its vibrational ground state are simply expressed as $\sigma_{if}^{FC}(R_{AB,eq})$—i.e., cross sections (18) evaluated at the internuclear equilibrium distance.

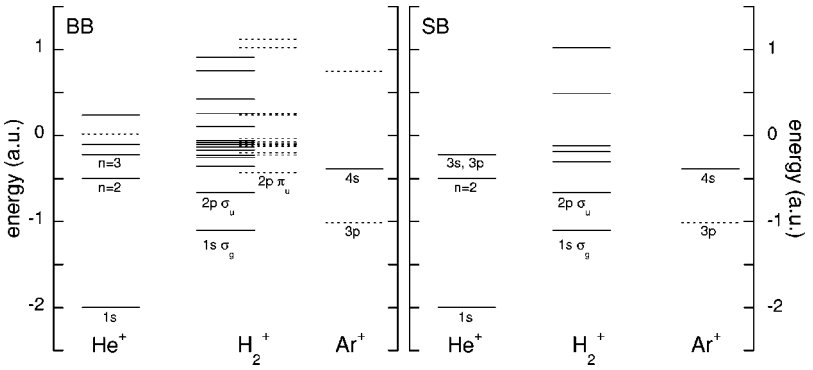

FIG. 2. Energy diagrams for the two projectiles and the hydrogen molecular ion (at the equilibrium internuclear distance $R_{AB,eq}=2$ a.u.). The spectra shown are obtained from the two basis sets BB and SB used in the semiclassical calculations. The two sets include some atomic and molecular pseudo states. p and π states are shown by dashed lines.

III. RESULTS AND DISCUSSION

A. Models of the collision systems

The results which are presented in the following are based on the two methods described above that we have coded for use on workstations and parallel machines. They concern the study of two similar collision systems $He^{2+}/Ar^{2+}-H_2^+$, especially focusing on total capture [36]

$$He^{2+}/Ar^{2+} + H_2^+(1s\sigma_g) \rightarrow He^+/Ar^+ + H^+ + H^+. \quad (20)$$

For He^{2+} projectile all interactions are Coulombic while for Ar^{2+} we use the one-parameter model potential

$$V^{Ar^{2+}}(r) = -\frac{2}{r} - 16\frac{e^{-\beta r}}{r}\left[1+\frac{\beta}{2}r\right] \quad (21)$$

to describe the interaction between the active electron and Ar^{2+}.

1. Classical model

The classical cross sections are based on calculations including typically from 10 000 to 50 000 trajectories (initial conditions) to get statistical errors lower than 3% for all velocities. The initial conditions for the target correspond to the ones listed in [38], before random rotations of both the electron position and momentum and the molecule internuclear vector. The initial and final positions of the projectile on its trajectory are set large enough (typically 100 a.u. far from the target) such that the interactions between the two collision partners become negligible. It is also necessary to have enough simulation time to be able to detect the possible dissociation of H_2^+, a process which is at least one order of magnitude slower than the electron dynamics. As in standard CTMC calculations, the impact parameter b of each trajectory is chosen by taking randomly b^2 between 0 and b_{max}^2, where b_{max}, which depends on the impact velocity, is the largest impact parameter beyond which only elastic scattering occurs.

2. Semiclassical model

To describe the H_2^+ target, we diagonalize the Born-Oppenheimer Hamiltonian onto two different basis sets: (i) the first containing only σ states which are expanded in 16 STO's and (ii) the second with both σ and π states described, respectively, by 24 and 14 STO's. The first set has been optimized for all internuclear distances needed in our calculations (0.4–8 a.u.). The second and much larger basis set has been optimized only for the equilibrium distance $R_{AB,eq}=2$ a.u. to test the quality of the first, tractable, set. Only differences of the order of 0.1% or below have been observed for the energies of the ground and excited H_2^+ states of importance. Figure 2 shows schematically the energy diagrams corresponding to these two sets.

The He^+ capture states have been obtained by diagonalization onto the exact hydrogenic STO's: one set includes only the exact $n=1,2$ and $3s,3p$ states (i.e., 6 STO's for $\ell=0$ and 3 STO's for $\ell=1$), the other including also the exact $3d$ plus the pseudostates stemming from the diagonalization procedures; cf. Fig. 2.

Since the charge of the projectile, more than its internal electronic structure, was our interest, we have decided to use a simple, though crude, one-electron model for the Ar^+ capture states. The interaction between the frozen $1s^22s^22p^63s^23p^4$ configuration and the active electron was described by a model potential; cf. Eq. (21). With $\beta=3.4816$, we have obtained the energy of the ground state ($3p^5\,^2P$, named $3p$ in the following) equal to the exact value of -1.015 a.u. [59]. We have included the second doublet state, corresponding to $3p^44s\,^2P$ (named $4s$ in Fig. 2), with an energy equal to -0.387 a.u., 0.5% off the tabulated value [59]. An extra pseudostate obtained from the diagonalization of the $3p$ is also included in the basis BB; cf. Fig. 2.

In summary, we have constructed two basis sets, called SB and BB in Fig. 2, to perform our coupled-channel calculations. The minimal basis SB including the dominant and some minor channels was used for most of the computations. The larger basis set BB including up to 50 atomic and σ, π-molecular states was used to check the convergence of the SB representation; cf. next section.

We finally note that since the states included in the basis sets are fitted by GTO's to compute some of the matrix elements we have performed several checks of the numerical stability of our results by changing the quality of the fits (numbers of GTO's included, exponents of the GTO's) and no significative difference has been obtained.

B. Results

In Fig. 3 we present the total capture cross sections based on the classical method. Good agreement with experiments is observed in the high-energy side of the scale: slightly lower

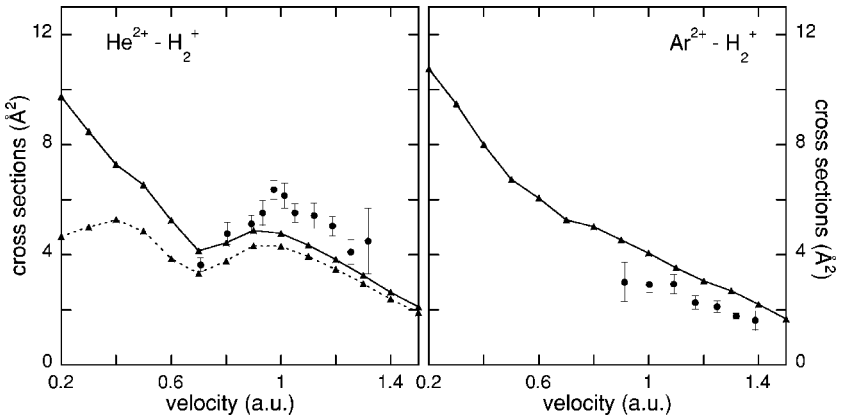

FIG. 3. Capture cross sections vs impact velocity for the two projectiles He^{2+} (left) and Ar^{2+} (right). The solid lines are the results from the classical model, and the dotted line shows the same cross sections excluding the unphysical resonant capture channels for the He^{2+} projectile; cf. text. The data marked by solid circles and error bars are the experimental results from Bräuning *et al.* [36].

for the He^{2+} projectile and higher for the Ar^{2+} projectile. The increase of the cross sections for decreasing velocities for the Ar^{2+} is reasonable since this trend is the signature of a near-resonant electron transfer channel, which is the dominant $Ar^+(3p)$ capture channel; cf. Fig. 2. For the He^{2+} projectile it is, however, not the case and the cross sections rise also in the low-energy region where there are unfortunately no measurements. The two-atom model presented in [36] gives there the expected decrease. A reason for the low-energy increase for He^{2+} is the classically allowed resonant capture which does not correspond to any physical quantum states: classically, at low energy, a large number of trajectories tend to transfer the electron without significant energy change, increasing artificially the capture cross sections. We have tested this assumption by removing the trajectories reaching this quantum mechanically forbidden region: i.e., trajectories which end up with the active electron bound to the He^{2+} nucleus with an energy lying between −2 a.u. and −0.5 a.u. (predominantly about −1 a.u. in the actual calculations). To do that we have used the correspondence criterion derived by Becker and MacKellar [60]:

$$\left[\left(n-\frac{1}{2}\right)(n-1)n\right]^{1/3} < n_c \leqslant \left[n\left(n+\frac{1}{2}\right)(n+1)\right]^{1/3}, \tag{22}$$

where $n_c = Z\sqrt{-2\epsilon_i}$ is a *classical n* level obtained from the classical binding energy $\epsilon_i < 0$: for $Z=2$ and $n=1$, the K shell corresponds to the range $\epsilon_K < -0.96$ a.u. Note that the use of this criterion does exclude the incriminated trajectories but also the possibility for capture into the K shell of He^+, which is, however, a very weak channel. Following this procedure the cross sections are indeed depleted at low impact velocities, as shown as the dotted line in Fig. 3 (left). The absence of resonant channels thus limits the applicability of the classical method for He^+ projectiles.

We now turn to the results from the coupled-channel approach. As a first step, we present in Fig. 4 the angular dependency of the integrals [61],

$$G(\theta,\varphi) = \int_0^{+\infty} bdbP_{capt}(b,R_{AB},\theta,\varphi), \tag{23}$$

for total capture in He^+-H_2^+ and $v=1.0$ a.u, $R_{AB}=R_{AB,eq}$. The results are based on calculations using the large basis set BB. In this figure, we note the constant value, which appears to be the lowest limit of G, for $\theta=0$—i.e., when the molecular axis is aligned parallel to the projectile beam. On the other hand, the curve for $\theta=90°$ corresponds to the upper limit of the G function. This tendency is in qualitative agreement with the experimental results of Reiser, Cocke, and Bräuning [62], showing for doubly charged projectiles and somewhat lower velocities that the capture process is favored when the molecular axis is perpendicular to the projectile beam.

Figure 4 shows indirectly also the complexity of the calculations to obtain the averaged cross sections; cf. Eqs. (17) and (18). For this figure, we have performed the calculations for 40 different molecular orientations. This task is only possible for tests with computer power of today, and certainly

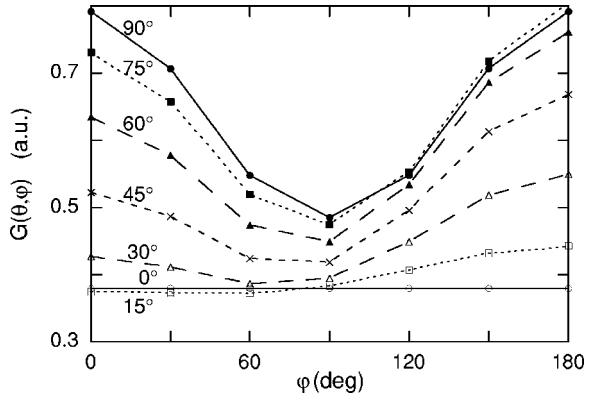

FIG. 4. He^{2+}-H_2^+ collision system at $v=1$ a.u. The orientation dependencies of the G integrals for total capture (evaluated at equilibrium internuclear distance $R_{AB,eq}=2$ a.u.), as function of the azimuthal angle φ and for different values of θ: 0°, 15°, 30°, 45°, 60°, 75°, and 90°.

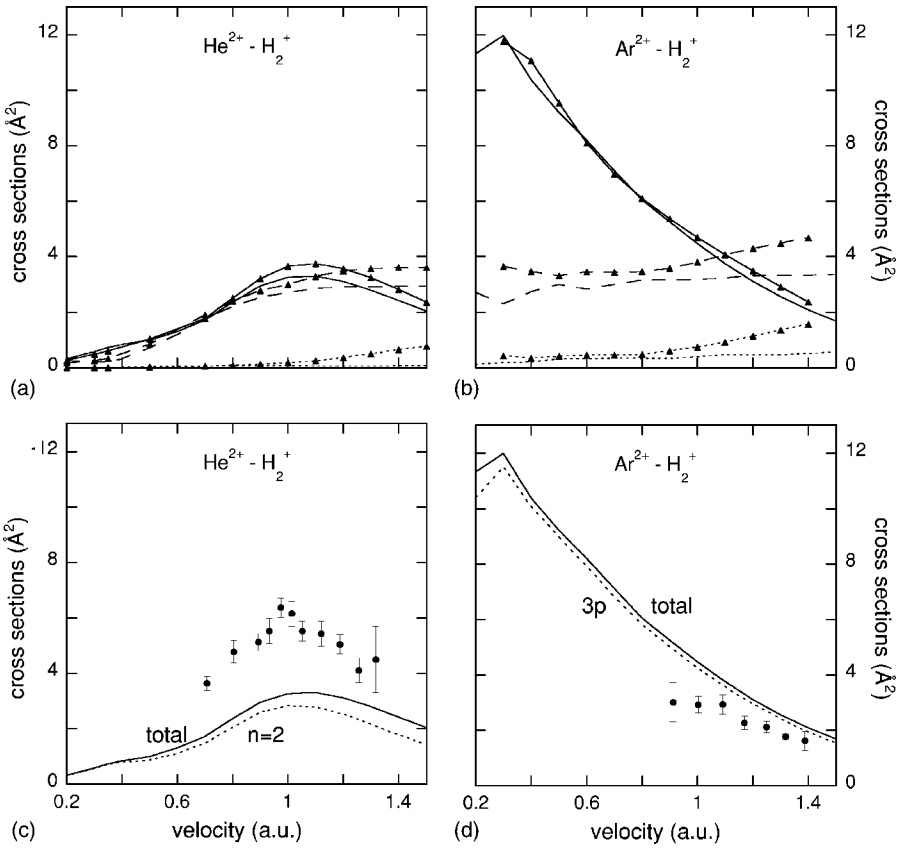

FIG. 5. Cross sections, calculated with the semiclassical model, as function of the impact velocity for the two collision systems He^{2+}-H_2^+ (left) and Ar^{2+}-H_2^+ (right). The upper panels [(a) and (b)] display the cross sections for capture (solid lines), excitation (dashed lines), and ionization (dotted lines). The lines marked with triangles show the results obtained with the large basis set BB while the others stems from the SB basis set. The lower panels [(c) and (d)] compare the total capture cross sections to the experimental data from Bräuning *et al.* [36]. The dotted lines display the cross sections for the dominant capture channels—i.e., $He^+(n=2)$ for He^{2+}-H_2^+ and $Ar^+(3p)$ for Ar^{2+}-H_2^+.

not for a large basis set and many velocities and internuclear distances. We have therefore chosen to compute orientation averaged cross sections using only three orientations corresponding to the axes x,y,z:

$$\sigma_{if}(R_{AB}) = \frac{2\pi}{3}[G_{if}(\pi/2,0) + G_{if}(\pi/2,\pi/2) + G_{if}(0,0)]. \tag{24}$$

In the case shown in Fig. 4, this approximation gives a capture cross section of about 3.47 Å while the integration over the 40 orientations gives 3.43 Å. In general the difference is not more than 5% [49], so this approximation may be considered as safe [57]. All cross sections presented in the following will be based on this procedure.

Cross sections based on the semiclassical method are displayed in Fig. 5 for both collision systems [63]. The upper panels [(a) and (b)] show the cross sections for capture, excitation, and ionization based on calculations with the large (BB) and medium (SB) basis sets. As expected capture is very important at low velocities for the near resonant Ar^{2+} system. On the other hand, for the He^{2+} projectile capture is not resonant and never exceeds significantly excitation. In fact, as a detailed dynamical study has exposed [49], capture and excitation are intimately coupled processes for this system. Moreover, for both collision systems the ionization mechanism is rather weak. In Fig. 5 we see also that the two basis sets produce somewhat different results, especially for ionization, but the capture cross sections are rather insensitive to the basis sets ($<10\%$). The basis set SB which allows large-scale computations at reasonable cost is expected to be

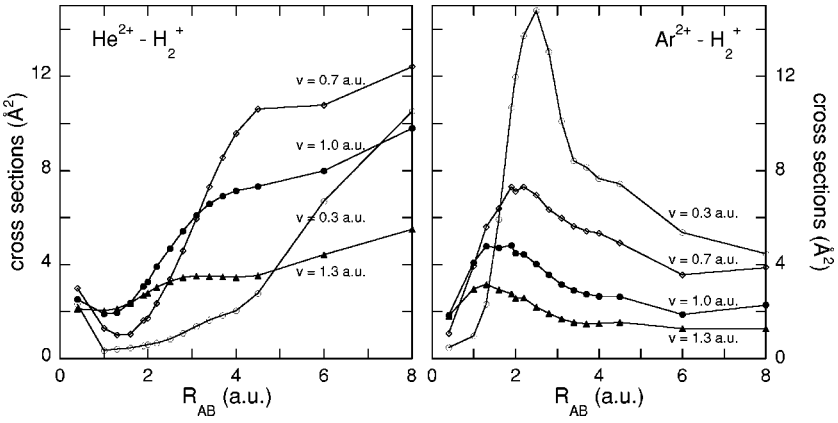

FIG. 6. Total capture cross sections as function of the H_2^+ internuclear distance R_{AB} for the two projectiles He^{2+} (left) and Ar^{2+} (right) and for four typical impact velocities $v=0.3$, 0.7, 1.0, and 1.3 a.u.

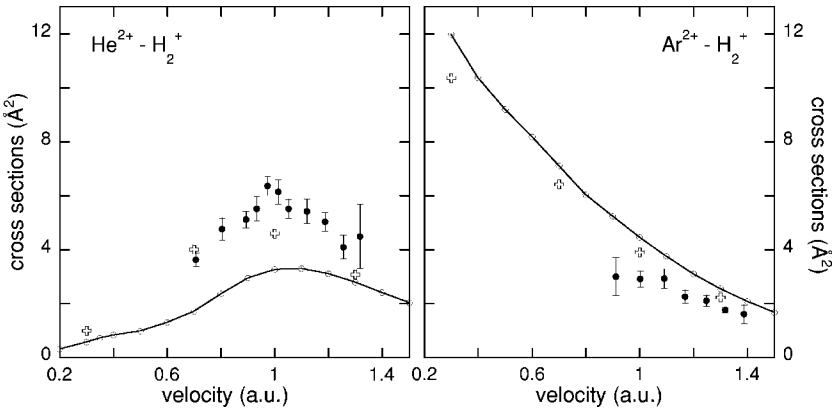

FIG. 7. Total capture cross sections vs impact velocity for the two projectiles He^{2+} (left) and Ar^{2+} (right). Solid circles: experimental data from Bräuning *et al.* [36]. Solid lines: semiclassical results assuming an initial H_2^+ vibrational ground state (as in Fig. 5). Open crosses: semiclassical results assuming a Franck-Condon initial vibrational distribution; cf. text.

converged enough and to give correct cross sections for the last part of our discussion. In the lower pannels of the figure [(c) and (d)] we only consider the capture results in more details and in comparison with the experimental results of [36]. First of all we see that the most dominant final channels are the $n=2$ level and the $3p$ states for He^{2+} and Ar^{2+} collisions, respectively. Furthermore, the general trend of both measurements are again reproduced. For Ar^{2+} the theoretical results overestimate the experimental cross sections and are in excellent agreement with the classical results of Fig. 3. For He^{2+} the calculations, in contrast to the classical calculations, reproduce now the general experimental trend in the whole energy range, but the absolute magnitude is lower than the data in [36]. These systematic differences cannot be explained by neither statistical experimental uncertainties nor basis convergence failures.

However, in the experiment, the molecular ions are created by ECR sources in excited vibrational states. Since no vibrational cooling scheme (e.g., low-energy electron-induced deexcitation [64]) has been applied in the experimental procedure of [36], one has to assume an initial distribution over the vibrational states of H_2^+ in its electronic ground state. For comparison, the capture cross sections should then be averaged as

$$\overline{\sigma_{capt}} = \sum_{\nu} A_{\nu} \sigma_{capt}^{(\nu)}, \tag{25}$$

where the vibrational distribution coefficients A_ν are unknown from the experimental point of view and $\sigma_{capt}^{(\nu)}$ correspond to the cross sections defined in Eq. (19), summed over all capture channels. The theoretical determination of the $\sigma_{capt}^{(\nu)}$ cross sections for large values of the vibrational quantum numbers (typically up to $\nu=10$) requires knowledge of $\sigma_{capt}(R_{AB})$ in a wide range of molecular internuclear distances.

The dependence of the capture cross sections, computed with the SB basis set, upon H_2^+ internuclear distance is presented in Fig. 6 for both collision systems and for four different velocities. The figures display clear differences between the two systems. For the He^{2+} projectile the cross sections are minimal around the equilibrium internuclear distance and increase steadily for increasing R_{AB}. This is related to the decrease of the Q value for the dominant capture $He^+(n=2)$ channels, the $1s\sigma_g$ ground-state energy rising significantly to reach resonance asymptotically ($R_{AB}\rightarrow\infty$). If highly excited vibrational states are involved in the experimental procedure, large values of R_{AB} become important. This dependence does explain the underestimation of the cross sections evaluated at the equilibrum distance. For Ar^{2+} the cross sections behave very differently with the internuclear distance: capture is strongest around equilibrium and decreases significantly, especially for our lowest velocity. As mentioned before, capture to the $Ar^+(3p)$ states is resonant around $R_{AB,eq}$ and the Q value increases on both sides, resulting in "bell-shaped" cross sections. In this case, the possible initial vibrational excitation of the molecular target is expected to reduce the capture cross sections by increasing the weigth of the large internuclear distance region.

As an illustration we have evaluated $\overline{\sigma_{capt}}$ for a few typical velocities, assuming that the A_ν of Eq. (25) are the Franck-Condon factors given in [65]—that is, assuming the sudden formation of H_2^+ from H_2. These results are presented in Fig. 7 with open crosses, together with the experimental data of [36] and the theoretical results assuming vibrational ground state (as in Fig. 5). For He^{2+} the results show an increase of the cross sections to a very reasonable agreement with the experimental data. On the other hand, for Ar^{2+}, the averaging procedure decreases the cross sections as expected from Fig. 6 but this effect is minimal. All in all the results taking into account the initial vibrational excitation of the target in Fig. 7 show indeed an important improvement in the agreement between theory and experiment, and give a strong indication on the vibrational distribution of the H_2^+ beam. From these results one may even assume a higher vibrational excitation than the ones given by the Franck-Condon factors: these latter are peaked around $\nu=2$ and a shift to higher vibrational quantum numbers would amplify the increase of the cross sections for He^{2+} projectile and their decrease for the Ar^{2+}. In future generations of collision experiments involving H_2^+, the vibrational state (or distribution) would be important to control.

IV. CONCLUSION

In conclusion, we have developed and implemented a nonperturbative semiclassical method to describe inelastic electronic processes in collisions between ions and molecules. We have presented a first application of the method to

calculations of charge transfer cross sections for α particles and Ar^{2+} colliding with H_2^+. The coupled-channel results are compared with experimental data and classical calculations. The agreement between both theoretical methods is surprisingly good. However, comparison with experiments shows systematic differences for both collision systems when H_2^+ is considered in its vibrational ground state. We have shown that the capture cross sections depend strongly on the internuclear distance and improving agreement was achieved when assuming a vibrational excitation of the molecular target, prior to the scattering stage. It was demonstrated that the initial vibrational distribution could be inferred from capture cross-section measurements. We have also presented orientation effects for electron capture. These effects which seem to be of general trend in ion-molecule scattering are in agreement with recent experimental studies.

ACKNOWLEDGMENTS

J.C. and A.D. acknowlegde support from the Bergen Computational Physics Laboratory (BCPL). The Laboratoire de Chimie Physique-Matière et Rayonnement is UMR 7614 du CNRS.

[1] W. J. van der Zande, W. Koot, D. P. de Bruijn, and C. Kubach, Phys. Rev. Lett. **86**, 1219 (1986).
[2] D. Dhuicq and V. Sidis, J. Phys. B **20**, 5089 (1987).
[3] G. Lubinski, Z. Juhász, R. Morgenstern, and R. Hoekstra, Phys. Rev. Lett. **86**, 616 (2001).
[4] T. Kusakabe, S. Satoh, H. Tawara, and M. Kimura, Phys. Rev. Lett. **87**, 243201 (2001).
[5] P. Sobocinski *et al.*, J. Phys. B **35**, 1353 (2002).
[6] A. Lafosse, J. C. Houver, and D. Dowek, J. Phys. B **35**, 819 (2001).
[7] I. Ben-Itzhak *et al.*, J. Phys. B **29**, L21 (1996).
[8] C. McGrath, M. B. Shah, P. C. E. McCartney, and J. W. McConkey, Phys. Rev. A **64**, 062712 (2001).
[9] B. Siegmann *et al.*, Phys. Rev. A **66**, 052701 (2002).
[10] W. Wolff *et al.*, Phys. Rev. A **65**, 042710 (2002).
[11] R. D. DuBois *et al.*, Phys. Rev. A **62**, 060701 (2000).
[12] M. Saito *et al.*, J. Phys. B **36**, 699 (2003).
[13] N. Stolterfoht *et al.*, Phys. Rev. Lett. **87**, 023201 (2001).
[14] L. Nagy, L. Kocbach, K. Pora, and J. P. Hansen, J. Phys. B **35**, L453 (2002).
[15] G. Laurent *et al.*, J. Phys. B **35**, L495 (2002).
[16] Direct studies are also possible through initial preparation of oriented molecules by laser pumping techniques—e.g., H. Sakai *et al.*, Phys. Rev. Lett. **87**, 083001 (2003); M. Machholm and N. E. Henriksen, *ibid.* **87**, 193001 (2001).
[17] S. A. Synnes, F. Søraas, and J. P. Hansen, J. Atmos. Sol.-Terr. Phys. **60**, 1695 (1998).
[18] S. L. Mielke *et al.*, Phys. Rev. Lett. **91**, 063201 (2003).
[19] G. A. Parker *et al.*, J. Chem. Phys. **117**, 6083 (2002).
[20] D. H. Zhang, D. Xie, M. Yang, and S.-Y. Lee, Phys. Rev. Lett. **89**, 283203 (2002).
[21] E. A Gislason, G. Parlant, and M. Sizun, in *State Selected and State to State Ion-Molecule Reaction Dynamics*, edited by M. Baer and C. Y. Ng (Wiley, New York, 1992), Pt. 2, pp. 321–421.
[22] N. Marković and G. D. Billing, Mol. Phys. **98**, 1771 (2000).
[23] M. Kimura, S. Chapman, and N. F. Lane, Phys. Rev. A **33**, 1619 (1986).
[24] B. H. Bransden and M. R. C. McDowell, *Charge Exchange and the Theory of Ion-Atom Collisions* (Clarendon, Oxford, 1992).
[25] L. F. Errea *et al.*, J. Phys. B **32**, 1705 (1999).
[26] M. Kimura *et al.*, Phys. Rev. A **61**, 032708 (2000).
[27] R. Shingal and C. D. Lin, Phys. Rev. A **40**, 1302 (1989).
[28] Y. D. Wang and J. H. McGuire, Phys. Rev. A **44**, 367 (1991).
[29] W. Fritsch, Phys. Rev. A **46**, 3910 (1992).
[30] F. Sattin and L. Salasnich, Phys. Scr. **58**, 464 (1998).
[31] C. Illescas and A. Riera, J. Phys. B **31**, 2777 (1998).
[32] R. E. Olson and C. R. Feeler, J. Phys. B **34**, 1163 (2001).
[33] C. L. Kirschbaum and L. Wilets, Phys. Rev. A **21**, 834 (1980).
[34] W. A. Beck and L. Wilets, Phys. Rev. A **55**, 2821 (1997).
[35] J. S. Cohen, Phys. Rev. A **59**, 1160 (1999).
[36] H. Bräuning *et al.*, J. Phys. B **34**, L321 (2001).
[37] J. S. Cohen, Phys. Rev. A **51**, 266 (1995).
[38] J. S. Cohen, Phys. Rev. A **56**, 3583 (1997).
[39] R. E. Olson, Phys. Rev. A **27**, 1871 (1983).
[40] J. Lu, J. P. Hansen, S. E. Nielsen, and A. Dubois, J. Phys. B **31**, 3665 (1998).
[41] W. Fritsch and C. D. Lin, Phys. Rep. **202**, 1 (1991).
[42] Note that in Eq. (5) we have chosen the ETF's to dress only the projectile orbitals for simplicity and for coherence with Fig. 1. Due to the sudden approximation invoked in our model, these ETFs are two-center in nature and in Eq. (5) one could have distributed them on both the projectile center and the diatomic molecule center of mass. However, our choice in the expression of the scattering state does not affect the generality of the coupled differential equations (7), which are Galilean invariant [24].
[43] D. R. Bates and R. McCarroll, Proc. R. Soc. London, Ser. A **245**, 175 (1958).
[44] M. H. Beck, A. Jäckle, G. A. Worth, and H.-D. Meyer, Phys. Rep. **324**, 1 (2001) and references therein.
[45] D. Rapp and C. M. Chang, J. Chem. Phys. **57**, 4283 (1972).
[46] M. Gargaud and R. McCarroll, J. Phys. B **18**, 463 (1985).
[47] K. O-ohata, H. Taketa, and S. Huzinaga, J. Phys. Soc. Jpn. **21**, 2306 (1966).
[48] W. Hehre, R. F. Stewart, and J. A. Pople, J. Chem. Phys. **51**, 2657 (1969).
[49] J. Caillat, Ph.D. thesis, Université Pierre et Marie Curie, Paris, France 2003.
[50] J. P. Hansen and A. Dubois, Comput. Phys. Commun. **67**, 456 (1992).
[51] J. P. Hansen, Comput. Phys. Commun. **58**, 217 (1990).
[52] L. F. Errea, L. Méndez, and A. Riera, J. Phys. B **12**, 69 (1979).
[53] L. Kocbach and R. Liska, J. Symb. Comput. **25**, 367 (1998).
[54] L. F. Shampine and M. K. Gordon, *Computer Solution of Or-*

dinary Differential Equations: the Initial Value Problem (Freeman, San Fransisco, 1975).
[55] T. A. Green, Proc. Phys. Soc. London **86**, 1017 (1965).
[56] When the integration over all collision planes $(\vec{b},\vec{v})$ is performed, the φ dependence of the probabilities drops so that the integrations over this angle gets to a trivial 2π factor. Note that for convenience in our code, we have instead kept fixed the collision plane and turned the molecule around the *z* axis to calculate the azimuthal dependences; cf. Fig. 4.
[57] L. F. Errea *et al.*, J. Phys. B **30**, 3855 (1997).
[58] D. Elizaga *et al.*, J. Phys. B **33**, 2037 (2000).
[59] C. E. Moore, *Atomic Energy Levels*, Circ. Nat. Bur. Stand. No. 467 (U.S. Government Printing Office, Washington, DC, 1949), Vol. I.
[60] R. L. Becker and A. D. MacKellar, J. Phys. B **17**, 3923 (1984).
[61] These integrals do not correspond to cross sections since they exclude the integration over the azimuthal angle but appear in the evaluation of any cross section; cf. Eqs. (17)–(19).
[62] I. Reiser, C. L. Cocke, and H. Bräuning, Phys. Rev. A **67**, 062718 (2003).
[63] In this section we present Franck-Condon-type cross sections, evaluated at $R_{AB,eq.}$. Few selective test calculations taking care of the initial vibrational ground-state distribution have been performed and did not show any significative differences in the cross sections.
[64] S. Krohn *et al.*, Phys. Rev. A **62**, 032713 (2000).
[65] D. Villarejo, J. Chem. Phys. **49**, 2523 (1968).